Received: 30 April 2020 | Revised: 5 July 2020 | Accepted: 28 July 2020
DOI: 10.1002/pip.3326

RESEARCH ARTICLE

PROGRESS IN PHOTOVOLTAICS WILEY

InGaN/GaN multi-quantum-well solar cells under high solar concentration and elevated temperatures for hybrid solar thermal-photovoltaic power plants

Gilad Moses[1,2] | Xuanqi Huang[3] | Yuji Zhao[3] | Matthias Auf der Maur[4] | Eugene A. Katz[1,5] | Jeffrey M. Gordon[1]

[1]Department of Solar Energy and Environmental Physics, Blaustein Institutes for Desert Research, Ben-Gurion University of the Negev, Sede Boqer Campus, 8499000, Israel

[2]Albert Katz School for Desert Studies, Blaustein Institutes for Desert Research, Ben-Gurion University of the Negev, Sede Boqer Campus, 8499000, Israel

[3]School of Electrical, Computer and Energy Engineering, Arizona State University, Tempe, AZ, 85287, USA

[4]Department of Electronic Engineering, University of Rome Tor Vergata, via del Politecnico 1, Rome, 00133, Italy

[5]Ilse Katz Institute for Nanoscale Science and Technology, Ben-Gurion University of the Negev, Be'er Sheva, 8410501, Israel

Correspondence
Eugene A. Katz and Jeffrey M. Gordon, Department of Solar Energy and Environmental Physics, Blaustein Institutes for Desert Research, Ben-Gurion University of the Negev, Sede Boqer Campus, 8499000, Israel.
Email: keugene@bgu.ac.il; jeff@bgu.ac.il

Abstract

Hybrid solar electricity generation combines the high efficiency of photovoltaics (PVs) with the dispatchability of solar thermal power plants. Recent thermodynamic analyses have shown that the most efficient strategy constitutes an integrated concentrating PV-thermal absorber operating at high solar concentration and at the high temperatures suitable to efficient commercial steam turbines (~673–873 K). The recuperation of PV thermalization losses and the exploitation of sub-bandgap photons can more than compensate for the inherent decrease of PV efficiency with temperature in properly tailored tandem solar cells for which promising candidates are III–N alloys. Recently, there have been considerable efforts to develop apposite InGaN solar cells by producing InGaN/GaN multiple quantum wells (MQWs) as the top cell in a tandem PV device that would absorb the short-wavelength regime of the solar spectrum, while sub-bandgap photons and PV thermalization are absorbed in the thermal receiver.

We present measurements of current–voltage curves and external quantum efficiency spectra for InGaN/GaN MQW solar cells under high sunlight intensity, up to 1 W/mm^2 (1000 suns) and elevated temperature, up to 723 K. We find that the short-circuit current increases significantly with temperature, while the magnitude of the temperature coefficient of the open-circuit voltage decreases with solar concentration according to basic photodiode theory. Conversion efficiency peaks at 623–723 K under ~300 suns, with no perceptible worsening in cell performance under extensive temperature and irradiance cycling—an encouraging finding in the quest for high-temperature high-irradiance cells.

KEYWORDS
concentrator photovoltaics, efficiency temperature coefficient, hybrid solar thermal-photovoltaic, InGaN/GaN, multiple quantum well

1 | INTRODUCTION

Essentially, all large-scale solar electricity production installed to date comprises one of two technologies: concentrated solar power (CSP) or photovoltaics (PVs). In CSP (5.5 GW$_{peak}$ installed as of 2018),[1] concentrated sunlight heats a collector fluid that then generates the steam used in conventional turbines. CSP *yearly-average* conversion efficiencies (~14–18%) are essentially the same as those achieved by

PV systems[2,3] and less than those reached by concentrating PV (CPV) plants (~30%).[4] Yearly-average efficiency—unlike efficiency under standard test conditions—subsumes cosine losses, shading losses, the dependence of efficiency on solar irradiance and collector temperature, and all losses in the turbine block (for CSP) or power conditioning (for PV and CPV). Moreover, the installed cost per peak watt and the levelized cost of electricity from CSP is considerably higher than for PV.[5] But PV power today is limited in its grid penetration by the lack of affordable and efficient storage technologies that can be realized worldwide. This refers not just to battery technologies but also to alternatives such as supercapacitors, compressed air, flywheels, and pumped hydro,[6,7] as well as to developing and implementing complementary control strategies for grid optimization.[7]

CSP remains viable because it can provide instantaneous power based on demand, via the use of gas-fired backup heating and/or high-temperature thermal storage. Currently, this is not the case for PV, the value of which is essentially reducing fuel consumption in existing conventional power plants. The major impact of PV is in utility-scale stations (~100–600 MW per installation): more than 500 GW by the end of 2018.[1]

The multijunction (MJ) III–V cells used in CPV comprise several monolithically stacked p–n junctions grown by gas-phase epitaxy, with tunnel junctions in the interfaces between the subcells. The bandgaps of the subcells are chosen for maximal utilization of the solar spectrum.

In order to simultaneously benefit from the dispatchability of CSP and the high efficiency of CPV, MJ concentrator cells can be integrated with CSP to create a hybrid CPV/CSP station.[8–11] The hybrid receiver exploits sub-bandgap photons and nominal PV thermalization losses to generate heat from which conventional steam turbines can be driven (Figure 1). Detailed modeling[8–11] has shown that this approach can yield a system efficiency that is superior to that of two separate CPV and CSP stations. The efficiency of the hybrid strategy turns out to be maximized for an approximately equal mix of CSP and

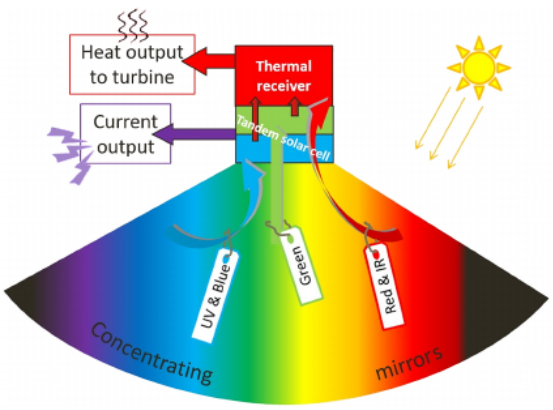

FIGURE 1 Schematic of an integrated CPV/CSP receiver in a hybrid solar power plant. The solar cells sit atop a thermal absorber and are thermally bonded to it, such that sub-bandgap photons and nominal thermalization losses from the PV cells are recuperated as high-temperature heat that contribute to driving steam turbines [Colour figure can be viewed at wileyonlinelibrary.com]

CPV, while using two-junction III–V cells with relatively high bandgaps.[8–11] For properly tailored cells, the efficiency loss for operating PV cells at elevated temperatures can be mitigated by the recuperation of the thermal losses.

One approach for both enhancing the efficiency of concentrator PV cells and diminishing the extent to which efficiency decreases with temperature is the incorporation of multiple quantum wells (MQWs).[12,13] Quantum wells can extend cell absorption at photon energies below the bandgap of the bulk host material and thereby can increase the current to a degree that more than compensates for any associated voltage loss. Research has been geared toward MQW cells with markedly greater carrier lifetimes and better carrier collection.[12,13] MQWs can be valuable in the subcells comprising MJ PVs because their bandgap can be tailored to near-optimal values while maintaining lattice-matching. Equally significant for this study is that the magnitude of the temperature coefficient of cell efficiency can be lessened considerably.[14–18]

III–N alloys are widely used in electronics and optoelectronics industries due to their unique optical and physical properties that include a high absorption coefficient, a wide range of bandgaps (0.64 eV for InN, 3.4 eV for GaN, 6.2 eV for AlN), thermal stability, and radiation resistance.[14–16] Recently, there have been concerted efforts to develop high-efficiency InGaN solar cells. One method to control the bandgap and achieve a high-quality material is to produce InGaN/GaN MQWs as the cell's absorbing layer. Making the InGaN/GaN layers a few nanometers thick helps avoid grain formation while improving material quality and PV performance.[16] These cells are promising for high-temperature hybrid solar thermal-PV power plants and as a power source for near-sun space missions.[14–18]

Previous studies on InGaN/GaN MQW solar cells presented temperature-resolved external quantum efficiency (EQE), temperature-resolved current density–voltage (I–V) curves under simulated 1-sun irradiation, and temperature-resolved photoluminescence,[14] but there have been no reports on their high-intensity behavior, most notably at high temperature.

Here, we report experimental measurements on high-bandgap InGaN/GaN MQW solar cells (an EQE spectral range of 300–460 nm)[14] at solar concentration levels up to 1000 suns and temperatures up to 723 K, each of which is varied independently. Our results demonstrate that efficiency deterioration at elevated temperatures can be avoided and even reversed by using concentrated sunlight. Because the bandgap decreases as temperature rises, more of the sun's spectrum is absorbed. Furthermore, extensive cycling of the cells over these broad ranges of temperature and solar irradiance did not produce a lessening of any of the PV performance parameters. Our results suggest that these cells can be promising candidates for the top subcell in a tandem PV of the hybrid CPV-CSP device.

2 | EXPERIMENTAL METHODS

The structure of the cells we fabricated (Figure 2) comprises a bottom n-GaN layer grown on a (0001) sapphire substrate, and a top p-GaN

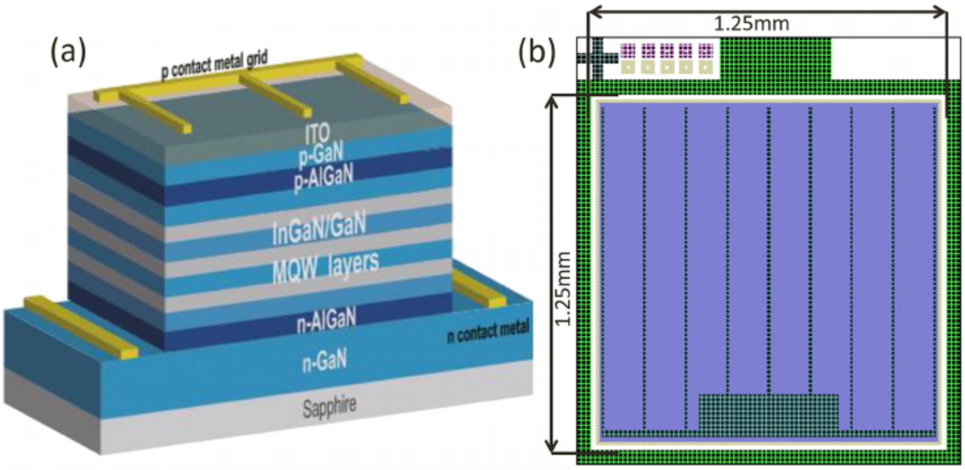

FIGURE 2 MQW cell structure schematics. (a) Cross section (reproduced from Huang et al.[14] with permission from the publisher). (b) Top view of the square cell. The active cell area is 0.9042 mm^2, which excludes the busbars, connecting pad, and metal fingers [Colour figure can be viewed at wileyonlinelibrary.com]

layer acting as the p–n junction, with a set of InGaN/GaN MQW layers acting as an absorption layer.[14] Five nm of n-AlGaN and five nm of p-AlGaN layers were included between the absorption layer and the doped GaN layers. Although the cell dimensions at the busbars are 1.25 × 1.25 mm (i.e., up to and including the white strips in Figure 2b), the active cell area, after deducting the area of the busbars, the connecting pad, and metal fingers, is only 0.9042 mm^2.

High-irradiance measurements were conducted in our fiber-optic minidish concentrator (Figure 3), comprising a dual-axis tracking parabolic dish that images the sun into an optical fiber (1.00-mm core diameter), which is threaded into the lab and used for assorted illumination modes of solar cells.[19,20] Solar radiation delivery is moderated by an iris on the concentrator's entry aperture. The fiber exit was in direct optical contact with the cell (Figure 3d). Hence, the ratio of active cell area (0.9042 mm^2) to illuminated cell area ($\pi \bullet (1.00)^2/4$ = 0.7854 mm^2) is 1.15. Cell temperature T was set with a ceramic heater designed for T up to 1273 K and controlled by a standard PID controller. The heater also served as a sample holder. Input solar power measurements were conducted with a spectrum-neutral pyrometric power meter (Ophir L30A detector with a Nova-II power meter), with readings taken before and after the I–V curve measurements and not in situ. All experiments were performed in our lab in Sede Boqer, Israel (latitude 30.8°N, longitude 34.8°E) during clear-sky periods within ±2 h around solar noon for which past measurements have shown the spectrum to be close to the AM1.5D standard spectrum.[20,21] Nonetheless, we directly measured the solar spectral irradiance with a StellarNet Black Comet fiber spectrometer that was calibrated with an Ocean Optics LS-1-CAL halogen lamp, presented in Figure S1 along with the AM1.5D spectrum.

Our measured I–V curves are plotted in Figure S2 from which the irradiance and temperature dependences of the principal performance variables plotted in Figures 4 and 5 were computed.

3 | RESULTS

Open circuit voltage (V_{oc}), short circuit current density (J_{sc}), fill factor (FF), and conversion efficiency η were determined at light intensities up to 990 suns and T up to 723 K (Figures 4 and 5). FF is defined as follows:

$$FF = \frac{P_{max}}{J_{sc} V_{oc}}, \quad (1)$$

where P_{max} is the electrical power density generated by the cell at its maximum-power point. Power conversion efficiency η is as follows:

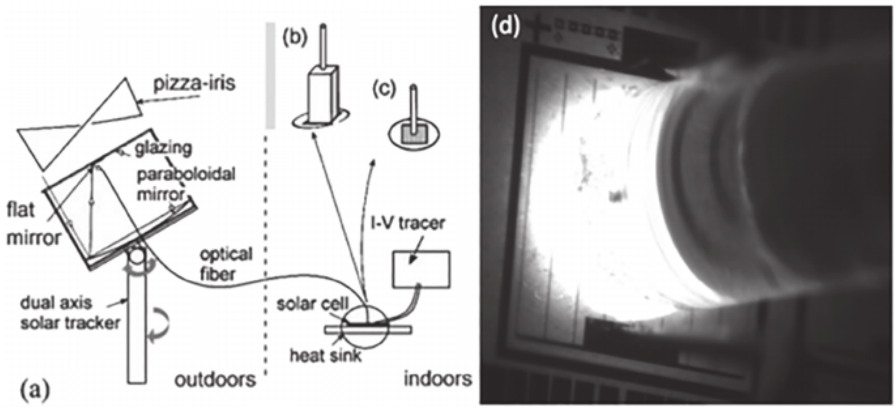

FIGURE 3 (a) Schematic of our fiber-optic minidish concentrator system. (reproduced from Katz et al.[19] with permission from the publisher.) (b) Optional use of a light homogenizer between the fiber and the cell. (c) Direct placement of the fiber tip on the cell (which was used for our experiments). (d) Photograph of the fiber tip (1.00-mm diameter) positioned on the MWQ cell

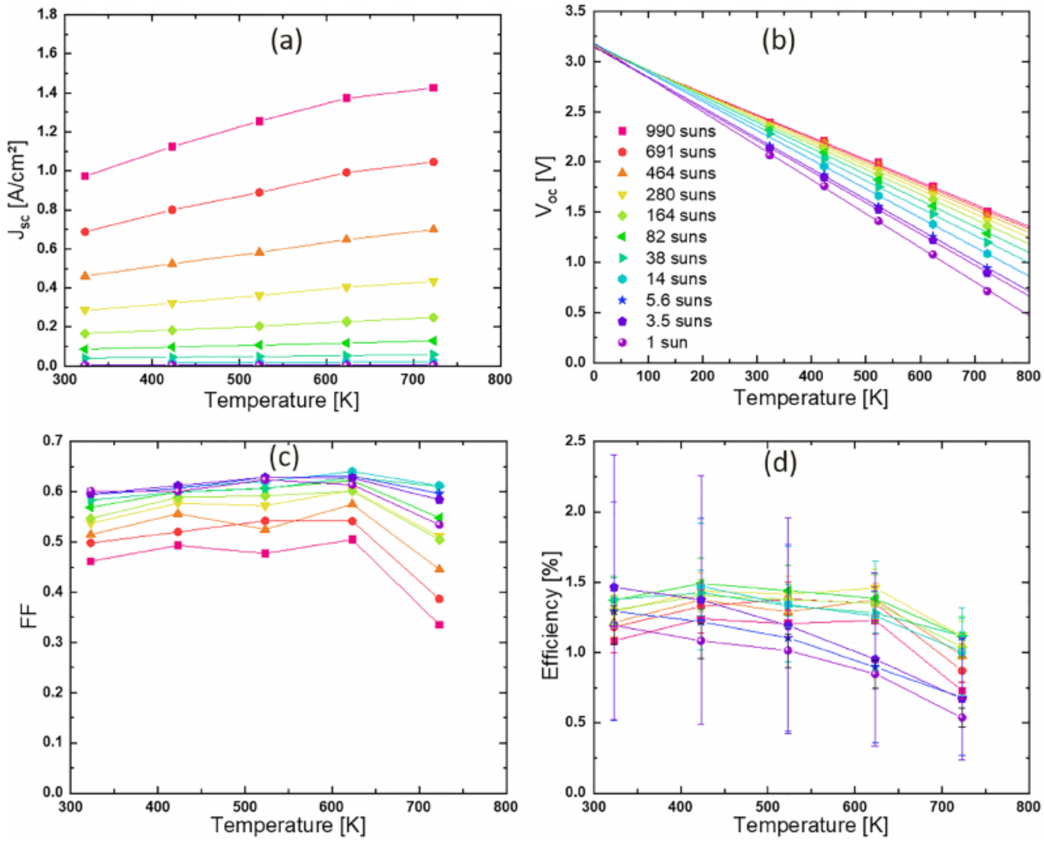

FIGURE 4 MQW cell parameters as a function of temperature. J_{sc} and efficiency data were corrected with Equation 3 as explained in the text. The legend of irradiance values in part (b) pertains to all four graphs [Colour figure can be viewed at wileyonlinelibrary.com]

$$\eta = \frac{P_{max}}{P_{in}} = \frac{J_{sc}V_{oc}FF}{P_{in}}, \quad (2)$$

where P_{in} is the input solar irradiance. The error bars in the voltage and current density measurements—and hence in FF—are smaller than the graph symbols. The error bars for the efficiency are relatively large due to the corresponding error bars for the solar power readings. The error bars in the power readings in Figure 5 are the standard deviations and are relatively large due mainly to the step motor of the tracker, but also subsume atmospheric changes during the day as well as power meter noise especially at low intensity values.

EQE measurements as a function of temperature are presented in Figure 6. The J_{sc} measured under high irradiance was noticeably below both (A) previously reported values[14] and (B) the value calculated from the standard AM1.5D solar spectrum based on EQE results. Toward understanding the reason for the discrepancy, the spectrum of the sunlight at the fiber exit was measured and compared with a direct sunlight measurement. The results displayed in Figure 7 show that, in the relevant spectral range for GaN MQW cells, the mirror and fiber combine to absorb a significant fraction of the light. J_{sc} was then recalculated at each temperature using the ratio between the EQE-weighted integrals based on the AM1.5D solar spectrum and the measured spectrum at the fiber exit:

$$J_{sc}(T,\text{corrected}) = \frac{\int_\lambda \lambda \cdot EQE_T(\lambda)\cdot AM1.5D(\lambda)\,d\lambda}{\int_\lambda \lambda \cdot EQE_{T}\cdot(\lambda)\cdot Minidish(\lambda)\,d\lambda} J_{sc}(T,\text{measured}), \quad (3)$$

where λ is the wavelength and $EQE_T(\lambda)$ is the measured EQE at temperature T. The $AM1.5D(\lambda)$ and $Minidish(\lambda)$ spectra were normalized so as to be equal at λ = 670 nm, such that the minidish spectral curve is always lower than the AM1.5D curve (as a consequence of concentrator and fiber attenuation). The two curves are then quite similar over the higher wavelength regime λ = 600–900 nm (the inset in Figure 7). In Figures 4 and 5, the 1-sun values of J_{sc} and conversion efficiency were measured in a solar simulator (Newport Oriel LCS-100, with a 91150-V calibration cell), whereas all other values, from our solar fiber-optic minidish, were corrected as explained above.

J_{sc} increased in proportion to solar concentration over the entire range of both concentration and temperature (Figure 5). Over most of the solar concentration range, J_{sc} increased linearly with temperature (below 691 suns—Figure 4), which stems from the bandgap decrease with temperature (Figure 6). Hence, as temperature is increased, more photons from the solar spectrum are absorbed. However, for the ultra-high concentration regime, J_{sc} starts to saturate above 573 K, which can be attributed to the observed deterioration of the EQE at high photon energy (Figure 6a) and merits further investigation. Polarization-free InGaN/GaN MQW solar cells (grown on a nonpolar

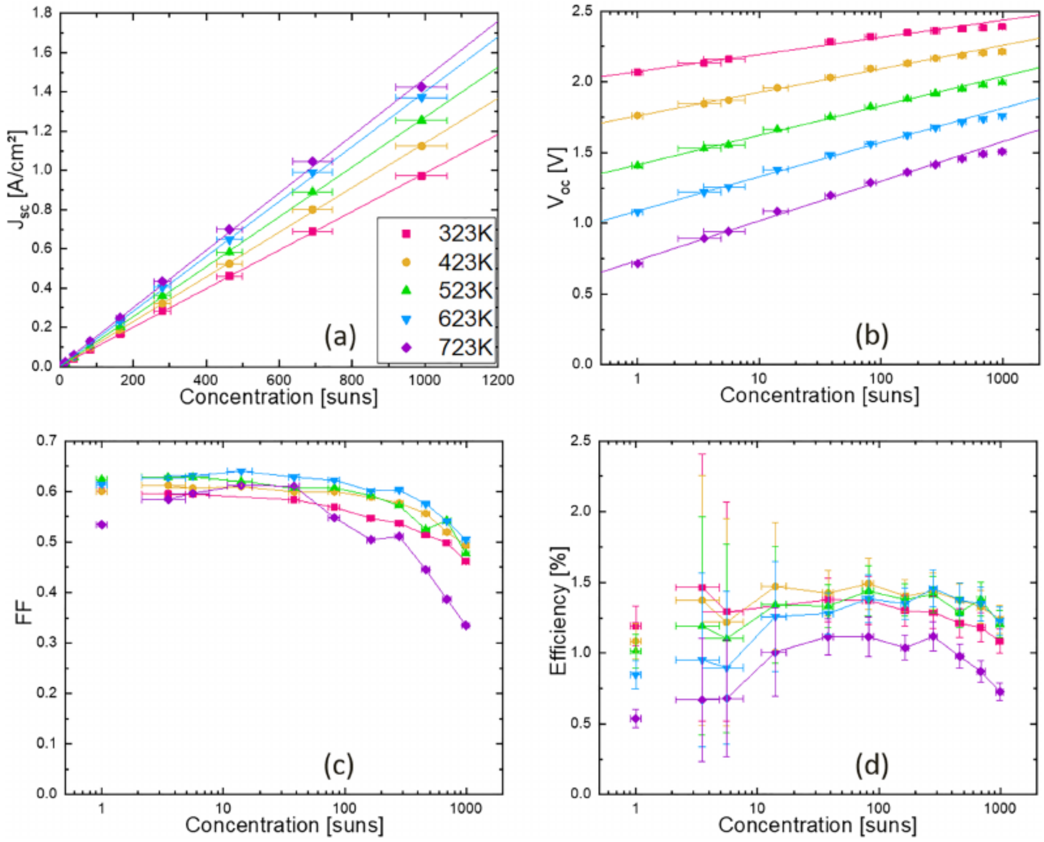

FIGURE 5 MQW cell parameters as a function of light intensity (1 sun = 1 mW/mm^2). J_{sc} and efficiency data were corrected with Equation 3 as explained in the text. The legend of temperature values in part (a) pertains to all four graphs [Colour figure can be viewed at wileyonlinelibrary.com]

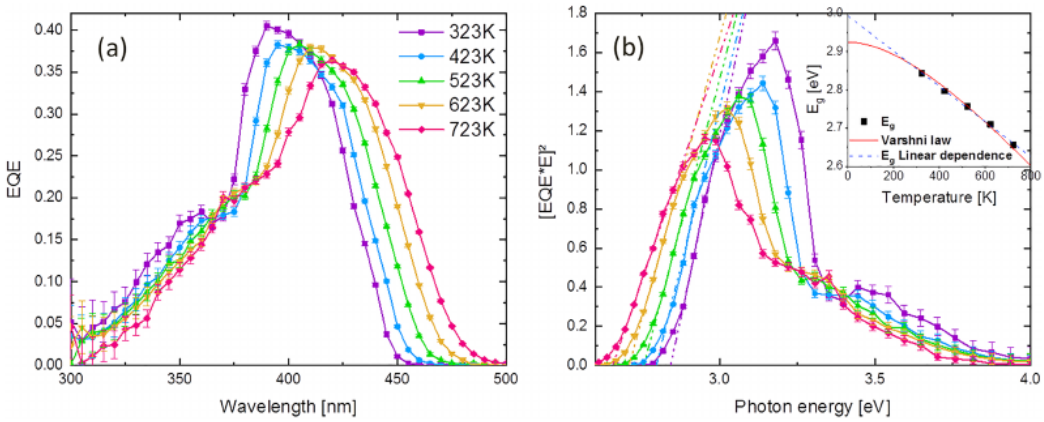

FIGURE 6 Measured external quantum efficiency (EQE) of the MWQ cell. (a) At different cell temperatures. (b) Calculation of bandgap energy E_g from EQE measurements based on the method of Leong et al.[22] The inset shows the computed E_g as a function of temperature (solid black squares) with a fit to both the Varshni law of Equation 5 (solid curve) and the corresponding linear approximation (dashed line). The legend of temperature values pertains to both graphs [Colour figure can be viewed at wileyonlinelibrary.com]

GaN substrate) have also been observed to exhibit an EQE that increases over the entire spectral range, which results in a superlinear increase of J_{sc} with temperature.[15]

V_{oc} decreased linearly with temperature (Figure 4) and increased logarithmically with light intensity (Figure 5), which is in accord with basic photodiode theory[24,25]:

$$V_{oc}(T) = a - bT = \frac{E_g}{q} - \frac{nkT}{q} \ln\left(\frac{C_o}{I_{ph}}\right), \tag{4}$$

where n is the diode quality factor, E_g is the bandgap energy, q is the elementary charge, k is the Boltzmann constant, I_{ph} is the photo-generated current, and C_o is a constant that depends on

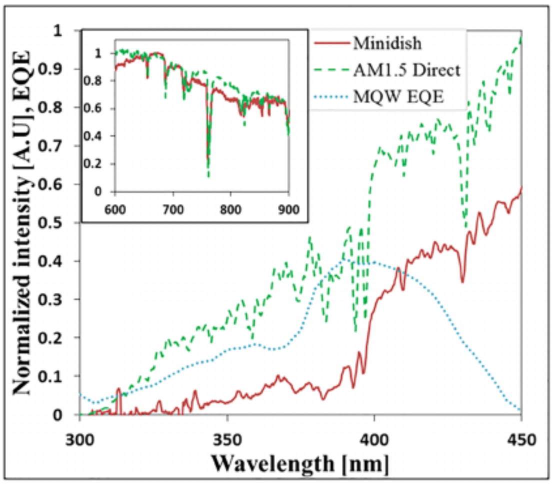

FIGURE 7 Comparison among spectra measured in the 300- to 450-nm wavelength band for our fiber-optic minidish concentrator, along with the low-wavelength tail of the AM1.5D solar spectrum[23] and the measured EQE of the InGaN/GaN MWQ solar cell. The inset shows good agreement over the long-wavelength tail [Colour figure can be viewed at wileyonlinelibrary.com]

material parameters. From the light intensity dependence of V_{oc} (Figure 5 , up to 300 suns), n = 2.00 ± 0.03 was regressed, indicative of nonradiative (Shockley–Read–Hall) recombination being the dominant recombination mechanism.

The slope b in Equation 4 is the temperature coefficient, which decreases when photocurrent increases, so the decrease of V_{oc} with temperature is smaller at higher solar concentration.[25,26] This was indeed observed over the entire range of solar concentration and temperature. Together with the increase in J_{sc}, it is among the main reasons that cell efficiency does not worsen as temperature is increased.

In an ideal solar cell, FF depends on V_{oc} only, so it should decrease slightly with temperature.[27] In practice, however, FF depends on series resistance losses, especially at high solar concentration.[19,20,28] As the trends plotted in Figures 4 and 5 reveal, a combination of these effects occurs, resulting in FF being maximized as a function of temperature and of solar concentration.

A particularly encouraging finding in the quest for PV cells for hybrid CPV/thermal solar power plants is the observed efficiency tolerance to elevated temperatures in the high-irradiance regime. Indeed, efficiency peaks at 623–723 K at a solar concentration of ~300 suns.

The small degree of nonuniformity in cell illumination (87% of the cell's active area was irradiated uniformly, with the remaining 13% in the dark) can give rise to a modest reduction in efficiency at high flux concentration (due to higher series resistance losses).[28] Although J_{sc} is basically independent of flux distribution, V_{oc} and FF are smaller than under uniform illumination. As shown in Katz et al.,[28] the cell can be approximately modeled as a parallel connection of two cells, one illuminated and the other in the dark. Hence, our results in the high-concentration regime may present efficiency values slightly below those that would be generated under uniform irradiation. The efficiency would peak at even higher solar concentration and temperature if cell series resistance could be reduced, for example, by decreasing the distance between the bottom electrodes in the cell (Figure 2a) and by improving the conductivity of p-GaN layers.

In Equation 4, the parameter $a = V_{oc}(T = 0\text{ K})$ is an activation energy of recombination, one of the fundamental parameters that describes photogeneration and recombination in a PV device. For a classical semiconductor solar cell, it should coincide with the material bandgap. Linear extrapolation to T = 0 K of the V_{oc} values measured at various solar concentration values converges to a single value: 3.157 ± 0.015 V.

The cell bandgap energy E_g was calculated from the fundamental edge of the EQE spectra according to the methods described in Leong et al. and Helmers et al.[22,29] and illustrated in Figure 6b. In the measured temperature range, E_g decreases with T by 0.5 meV/K, which is in good agreement with the published data for comparable semiconductors.[10,30] The inset in Figure 6bincludes the theoretical temperature dependence of the bandgap (the solid black curve), calculated for a bulk $In_{0.15}Ga_{0.85}N$ alloy (without strain) using Varshni's law[31]:

$$E_g(T) = E_g^0 - \frac{\alpha T^2}{\beta + T}, \tag{5}$$

where α and β are linearly interpolated between their respective values for pure GaN and InN, while E_g^0 is quadratically interpolated (including bandgap bowing[31]), that is,

$$E_g = xE_{g,InGaN} + (1-x)E_{g,GaN} - \varepsilon x(1-x), \tag{6}$$

with bowing parameter ε and indium concentration x. The calculated E_g^0 value of 2.92 eV (using α and β values taken from Vurgaftman and Meyer[31]) is more than 200 mV lower than that obtained by linear extrapolation of V_{oc} (Figure 4). However, the data plotted in the inset of Figure 6b show that the Varshni approximation of Equation 5 for E_g coincides with the linear approximation

$$E_g(T) = E_g^* - \gamma T, \tag{7}$$

in the temperature range of our measurements (the dashed line). This is also in agreement with similar behavior for other III–V solar cells.[32] Indeed, the linear extrapolation of E_g to 0 K (E_g^*) and the value of E_g^0 differ by less than 0.1 V. A detailed experimental and theoretical study of the behavior of V_{oc} in the low-temperature regime is beyond the scope of this paper and will be addressed in a future publication.

4 | CONCLUSIONS

Increasing sunlight intensity reduces the temperature coefficient of a solar cell, but for conventional solar cells, the conversion efficiency decreases with temperature even under high intensity. The results presented here reveal that in InGaN/GaN MQW solar cells, the conversion efficiency can *improve* with temperature at solar intensities of a few hundred suns. This stems from the current density increasing significantly with temperature, which compensates for the corresponding decrease in V_{oc} and *FF*. This property is essential for the use of such cells in a hybrid CPV/CSP receiver. We also note that the cells exhibited no perceptible performance penalty after numerous cycles of being exposed to the broad ranges of temperature and solar irradiance in our experiments.

Future work will focus on modifying cell materials and architecture in order to realize performance improvements, in particular, the reduction of cell series resistance. Another promising candidate is polarization-free MQW cells with an EQE that increases with temperature over the entire relevant spectral range.[15] Further research should also involve the search for a suitable bottom subcell of the tandem device envisioned for the hybrid solar receiver, as well as the experimental realization of such temperature-tolerant tandem PV devices.

ACKNOWLEDGEMENT

EAK is grateful for the visiting professor fellowship from the University of Rome Tor Vergata.

CONFLICT OF INTEREST

The authors declare that they have no known competing financial interests or personal relationships that could have appeared to influence the work reported in this paper.

ORCID

Gilad Moses https://orcid.org/0000-0003-1338-4659
Xuanqi Huang https://orcid.org/0000-0002-7085-4162
Jeffrey M. Gordon https://orcid.org/0000-0001-9180-5434

REFERENCES

1. REN21. *Renewables* 2019 Global Status Report. Renewable Energy Policy Network: Paris; 2019.
2. Zhang HL, Baeyens J, Degrève J, Cacères G. Concentrated solar power plants: review and design methodology. *Renew Sustain Energy Rev*. 2013;22:466-481.
3. Fraunhofer Institute for Solar Energy Systems. Photovoltaics report. Fraunhofer ISE: Freiburg, Germany; 2020.
4. Ghosal K, Lily D, Gabriel J, et al. Semprius field results and progress in system development. *IEEE J Photovolt*. 2014;4(2):703-708.
5. US Energy Information Administration. International Energy Outlook 2019. *Report #IEO2019*. US Department of Energy: Washington, DC; 2019.
6. Akbari H, Browne MC, Ortega A, et al. Efficient energy storage technologies for photovoltaic systems. *Solar Energy*. 2019;192:144-168.
7. Chen H, Cong TN, Yang W, Tan C, Li Y, Ding Y. Progress in electrical energy storage system: A critical review. *Prog Nat Sci*. 2009;19(3):291-312.
8. Vossier A, Zeitouny J, Katz EA, Dollet A, Flamant G, Gordon JM. Performance bounds and perspective for hybrid solar photovoltaic/thermal electricity-generation strategies. *Sustain Energy Fuels*. 2018;2(9):2060-2067.
9. Zeitouny J, Lalau N, Gordon JM, et al. Assessing high-temperature photovoltaic performance for solar hybrid power plants. *Sol Energy Mater sol Cells*. 2018;182:61-67.
10. Zeitouny J, Lalau N, Katz EA, et al. On the potential of solar cells to efficiently operate at high temperature. *AIP Conf Proc*. 2017;1881:080011.
11. Zeitouny J, Katz EA, Dollet A, Vossier A. Band gap engineering of multi-junction solar cells: effects of series resistances and solar concentration. *Sci Rep*. 2017;7(1):1766.
12. Barnham KWJ, Ballard I, Connolly JP, et al. Quantum well solar cells. *Physica E*. 2002;14(1-2):27-36.
13. Yanwachirakul W, Fujii H, Toprasertpong K, Watanabe K, Sugiyama M, Nakano Y. Effect of barrier thickness on carrier transport inside multiple quantum well solar cells under high-concentration illumination. *IEEE J Photovolt*. 2015;5(3):846-853.
14. Huang X, Chen H, Fu H, et al. Energy band engineering of InGaN/GaN multi-quantum-well solar cells via AlGaN electron- and hole-blocking layers. *Appl Phys Lett*. 2018;113(4):043501.
15. Huang X, Li W, Fu H, et al. High-temperature polarization-free III-nitride solar cells with self-cooling effects. *ACS Photonics*. 2019;6(8):2096-2103.
16. Bhuiyan AG, Sugita K, Hashimoto A, Yamamoto A. InGaN solar cells: present state of the art and important challenges. *IEEE J Photovolt*. 2012;2(3):276-293.
17. Williams JJ, McFavilen H, Fischer AM, et al. Refractory $In_xGa_{1-x}N$ solar cells for high-temperature applications. *IEEE J Photovolt*. 2017;7(6):1646-1652.
18. Williams JJ, McFavilen H, Fischer AM, et al. Development of a high-band gap high temperature III-nitride solar cell for integration with concentrated solar power technology. *Proc IEEE 43rd Photovoltaic Specialists Conference (PVSC)*. 2016;193-195.
19. Katz EA, Gordon JM, Feuermann D. Effects of ultra-high flux and intensity distribution in multi-junction solar cells. *Prog Photovolt Res Appl*. 2006;14(4):297-303.
20. Gordon JM, Katz EA, Feuermann D, Huleihil M. Toward ultrahigh-flux photovoltaic concentration. *Appl Phys Lett*. 2004;84(18):3642-3644.
21. Katz EA, Faiman D, Tuladhar SM, et al. *J Appl Phys*. 2001;90(10):5343-5350.
22. Leong WL, Ooi ZE, Sabba D, et al. Identifying fundamental limitations in halide perovskite solar cells. *Adv Mater*. 2016;28(12):2439-2445. https://doi.org/10.1002/adma.201505480
23. National Renewable Energy Laboratory, Golden, CO, USA. Reference Air Mass 1.5 Spectra|Grid Modernization|NREL; 2020. https://www.nrel.gov/grid/solar-resource/spectra-am1.5.html
24. Dupré O, Vaillon R, Green MA. *Thermal Behavior of Photovoltaic Devices*. Cham, Switzerland: Springer Int Publ; 2017.
25. Braun A, Katz EA, Gordon JM. Basic aspects of the temperature coefficients of concentrator solar cell performance parameters. *Prog Photovolt Res Appl*. 2013;21:1087-1094.
26. Braun A, Hirsch B, Vossier A, Katz EA, Gordon JM. Temperature dynamics of multijunction concentrator solar cells up to ultra-high irradiance. *Prog Photovolt Res Appl*. 2013;21(2):202-208.
27. Green MA. *Solar Cells: Operating Principles, Technology and System Applications*. Englewood Cliffs, NJ: Prentice-Hall Inc; 1982.
28. Katz EA, Gordon JM, Tassew W, Feuermann D. Photovoltaic characterization of concentrator solar cells by localized irradiation. *J Appl Phys*. 2006;100(4):044514.
29. Helmers H, Karcher C, Bett AW. Bandgap determination based on electrical quantum efficiency. *Appl Phys Lett*. 2013;103(3):032108.
30. Lorenz MR, Pettit GD, Taylor RC. Band gap of gallium phosphide from 0 to 900 k and light emission from diodes at high temperatures. *Phys Rev*. 1968;171(3):876-881.

31. Vurgaftman I, Meyer JR. Band parameters for nitrogen-containing semiconductors. *J Appl Phys*. 2003;94(6):3675-3696.
32. Mintairov MA, Evstropov VV, Mintairov SA, Shvarts MZ, Kalyuzhnyy NA. Dethermalization of carriers in GaAs solar cells with quantum objects. *Appl Phys Express*. 2019;12(3):035005.

SUPPORTING INFORMATION

Additional supporting information may be found online in the Supporting Information section at the end of this article.

How to cite this article: Moses G, Huang X, Zhao Y, Auf der Maur M, Katz EA, Gordon JM. InGaN/GaN multi-quantum-well solar cells under high solar concentration and elevated temperatures for hybrid solar thermal-photovoltaic power plants. *Prog Photovolt Res Appl*. 2020;28:1167–1174. https://doi.org/10.1002/pip.3326